Trop J Nat Prod Res, November 2025; 9(11): 5497 - 5510
ISSN 2616-0684 (Print)
ISSN 2616-0692 (Electronic)

Tropical Journal of Natural Product Research

Available online at https://www.tjnpr.org

Original Research Article

In Silico Evaluation of 3,6-Anhydro-D-Galactose from *Eucheuma denticulatum* Targeting Breast Cancer-Associated Molecular Pathways

Wa Ode N. Sari[1,2], Marhaen Hardjo[1,3], Syahrijuita[1,3], Ilhamuddin Azis[1,3], Ika Yustisia[1,3]*

[1]*Biomedical Sciences Program, Graduate School of Hasanuddin University, Makassar, South Sulawesi, Indonesia*
[2]*Universitas Muhammadiyah Kendari, Kendari, Southeast Sulawesi, Indonesia*
[3]*Department of Biochemistry, Faculty of Medicine, Hasanuddin University, Makassar, South Sulawesi, Indonesia*

ARTICLE INFO

Article history:
Received 24 July 2025
Revised 14 October 2025
Accepted 17 October 2025
Published online 01 December 2025

ABSTRACT

Breast cancer is a major global health concern, ranking among the leading causes of morbidity and mortality worldwide. Despite available therapies, drug resistance and side effects underscore the need for novel, safe, and effective treatments. Marine-derived bioactive compounds have attracted significant attention due to their diverse pharmacological properties, including anticancer activity. For example, 3,6-Anhydro-D-galactose (3,6-D-AHG), a monomer derived from the degradation of iota-carrageenan in the red macroalga *Eucheuma denticulatum*, has shown promising bioactivity. This study aimed to evaluate the anticancer potential of 3,6-D-AHG against breast cancer through a comprehensive *in silico* approach. Iota-carrageenan was extracted using microwave-assisted extraction, hydrolyzed to produce 3,6-D-AHG, and characterized by Fourier transform infrared (FTIR) spectroscopy. Computational analyses included ADMET profiling (AdmetLab 2.0), bioactivity prediction (PASS), protein target identification, network pharmacology analysis, gene expression profiling (GEPIA2), and molecular docking. FTIR spectroscopic data confirmed characteristic peaks of iota-carrageenan and 3,6-D-AHG at 1220-1260 cm^{-1} and 848-930 cm^{-1}, respectively. ADMET showed favorable pharmacokinetics, low toxicity, and compliance with Lipinski's rule, while PASS predicted a high probability of glucose oxidase inhibition. Key molecular targets identified were HK2, HSPA5, CA12, and LGALS3. Molecular docking showed a strong binding affinity of 3,6-D-AHG with HK2 and HSPA5 (–5.6 kcal/mol), exceeding that of D-glucose used as the control, suggesting disruption of cancer cell metabolism and stress response. In conclusion, 3,6-D-AHG is a promising candidate for breast cancer therapy. The results, although predictive, provide a strong rationale for further studies, supporting the potential of Indonesian marine resources as valuable sources of novel anticancer agents.

Keywords: *Eucheuma denticulatum*, 3,6-Anhydro-D-galactose, Breast cancer, Carrageenan, *In silico*.

Introduction

Cancer is a major global health challenge, contributing to high mortality rates and reduced life expectancy worldwide. According to the World Health Organization (WHO) in 2019, cancer ranked as the first and second leading cause of death before the age of 70 in 112 out of 183 countries.[1] The Global Cancer Statistics 2020 (GLOBOCAN) also stated that Indonesia ranked third to fourth among countries with the highest cancer-related deaths for ages 0–69. Breast cancer is the most prevalent cancer, with 66,271 new cases (16.2% of all cancer cases) and 22,598 deaths, ranking third among cancer-related causes of mortality.[2,3] These figures underscore the urgent need for effective, accessible, and safe therapeutic options as part of the national cancer control strategy. Current treatment modalities for breast cancer, including surgery, radiotherapy, and chemotherapy, are often limited by issues such as drug resistance, toxicity, and adverse side effects.[4,5]

*Corresponding author. E mail: ikayustisia@pasca.unhas.ac.id.
Tel.: +6282188120390

Citation: Sari WN, Hardjo M, Syahrijuita, Azis I, Yustisia I. *In Silico* Evaluation of 3,6-Anhydro-D-Galactose from *Eucheuma denticulatum* Targeting Breast Cancer-Associated Molecular Pathways. Trop J Nat Prod Res. 2025; 9(11): 5497 – 5510 https://doi.org/10.26538/tjnpr/v9i11.33

Official Journal of Natural Product Research Group, Faculty of Pharmacy, University of Benin, Benin City, Nigeria

This has led to the search for novel bioactive compounds with anticancer potential and minimal toxicity, particularly from marine natural resources, such as macroalgae.

Eucheuma denticulatum (ED) is one of the abundant red macroalgae species in Indonesian waters and has long been used as a source of carrageenan.[6] The extraction of ED carrageenan produces ιota-carrageenan, namely a sulfate polysaccharide consisting of 3,6-anhydro-D-galactose (D-AHG). The sulfate ester salt of D-galactose is connected by α-(1,3) and β-(1,4) linkages.[7] Over the past decades, polysaccharides from macroalgae have attracted attention in the biomedical field due to their broad biological activities such as anticoagulant, antitumor, antiviral, and immunomodulatory activities. In contrast to terrestrial plants, marine macroalgae cell walls naturally contain sulfated polysaccharides, which may play specialized roles in ionic regulation.[8]

In a previous study, carrageenan extracts from red macroalgae *Hypnea musciformis*, *Iridaea undulosa*, and *Eucheuma spinosum*, namely κ-, ι-, and λ-carrageenan types, were hydrolyzed using trifluoroacetic acid (TFA) at 60–80°C to produce oligosaccharides and disaccharides, including κ-carrabiose and ι-carrabiose. The oligosaccharides resulting from the hydrolysis partially showed improved cytotoxic activity with IC_{50} value approx. 0.074 ± 0.009 mg/mL for κ-oligosaccharides and 0.183 ± 0.015 mg/mL for ιota-oligosaccharides, suggesting that the breakdown of the heavy molecule can result in increased anticancer activity.[8] The compound 3,6-anhydro-α-D-galactose (D-AnG) has been identified as a unique product of *Kappaphycus alvarezii* hydrolysis and has potential biological activities, including induction of apoptosis in

ISSN 2616-0684 (Print)
ISSN 2616-0692 (Electronic)

MCF7 breast cancer cells by increasing the expression of the pro-apoptotic gene BAX and influencing cellular glucose uptake.[9] Consequently, the product from the hydrolysis of carrageenan has strong potential for the development of a natural antitumor agent with a mechanism of action that comprises disturbance of adhesion and inhibition of cancer cell metastasis.

Although, the anticancer potential of sulfated polysaccharides is well-documented, studies on D-AHG from ED and molecular interactions with breast cancer targets remain scarce. The mechanism of action has never been systematically investigated in an *in silico* model against breast cancer-associated proteins. This study applies molecular docking to predict the binding affinity and interaction profile of D-AHG with relevant molecular targets, offering a cost-effective and mechanistically informative approach for early-stage drug discovery. Therefore, the aim is to evaluate the anticancer potential of 3,6-anhydro-α-D-galactose from ED using *in silico* methods, focusing on interactions with breast cancer-related targets to support the development of novel, natural anticancer agents.

Materials and Methods

Chemicals

All analytical grade reagents were obtained from commercial suppliers and used without further purification. These included sulphuric acid (H_2SO_4, 98%, Merck KGaA, Darmstadt, Germany), ethanol (Merck KGaA, Darmstadt, Germany), purified water (OneMed, Indonesia), Benedict reagent (≥ 99% purity, ROFA Laboratory Centre, Indonesia), and D-galactose (≥ 99%, Sigma-Aldrich, St. Louis, MO, USA).

Collection and identification of macroalgae

Eucheuma denticulatum (ED) was supplied by seaweed farmers in Kolese village, Pasi Kolaga sub-district, Muna Regency, Southeast Sulawesi province, Indonesia. The macroalgae species were confirmed by marine botanists from the Faculty of Fisheries and Marine Sciences at Halu Oleo University, Kendari, Southeast Sulawesi, Indonesia.

Macroalgae preparation

A chilled container containing fresh ED was delivered to the Biochemistry Laboratory, Faculty of Medicine, Hasanuddin University in Makassar. The macroalgae were cleaned under running water, drained, and left to air-dry for five days before being weighed. The air-dried ED samples (1 kg) were further dried in an oven set at 50ºC. The oven-dried product (250 g) was pulverized using a grinder (FGD-Z300). The powdered sample was then sieved, and the ED flour obtained was sealed in a silica gel container until ready for use.

Microwave-assisted extraction (MAE) of macroalgae

About 20 grams of dry ED powder was macerated in 200 mL of 80% ethanol solution and then stirred with a magnetic stirrer at room temperature for 18 hours, then at 70°C for 4 hours to remove pigments, proteins, mannitol, and salts. After centrifugation at 6000 rpm for 15 minutes, the pellets obtained were dried. The dry pellets (0.23 g) were extracted in an EMM2308X Microwave (Electrolux, Stockholm, Sweden, manufactured in China with a rated power of 800 W, operating at 220 - 240 V/50 Hz) using distilled water as solvent at a ratio of 0.01 g dry ED powder to 100 mL water (1:10) for 5 minutes. The resulting extract was then centrifuged at 6000 rpm for 15 minutes. To the supernatant obtained (50 mL) was added 10 mL of 2% $CaCl_2$ (w/v), and left overnight at 4°C, and centrifuged again to remove the precipitated alginate sulfate polysaccharide,[10] in preparation for the next stage. The general workflow for the experimental procedure and *in silico* study is shown in Figure 1.

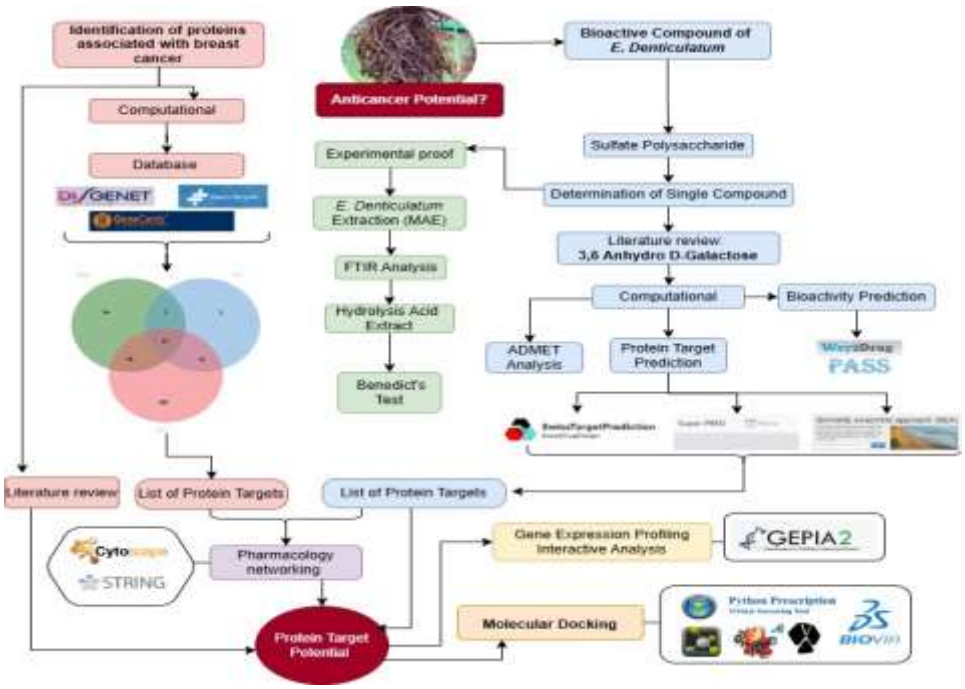

Figure 1: General workflow for the *in silico* study and experimental procedure

Acid hydrolysis of sulphated polysaccharide extract

About 10 mL of the solution of extracted polysaccharide sulfate from MAE procedure was placed into a 100 mL Erlenmeyer flask, and 20 mL of 0.2 M sulphuric acid (H_2SO_4) was added. The mixture was stirred for 5 minutes until homogeneous, and then heated in an autoclave at 121°C for 60 minutes. After the hydrolysis process, the filtrate was cooled and stored in sterile vials.[9]

Fourier transform infrared (FTIR) spectroscopic analysis

A total of 1 mL of ED polysaccharide sulfate was dried for 24 hours, crushed with 100 mg otassium bromide (KBr) until homogeneous to form thin pellets. Pellets were placed in the FTIR Spectrometer (IRPrestige-21, Shimadzu Corporation, Japan) sample compartment, and infrared spectra were recorded at wavenumber range of 4000 - 500 cm^{-1}, to identify the constituent functional compounds. A similar procedure was carried out on the hydrolysate obtained from the polysaccharide sulfate extract.[10]

Qualitative test for reducing sugars
About 0.5 mL of polysaccharide sulfate hydrolysate was placed into a test tube, and 0.5 mL of Benedict's reagent was added. The mixture was heated in a boiling water bath for 5 minutes, and the colour change was observed. The formation of green, yellow, orange, or brick red precipitates indicates the presence of reducing sugars in the sample, and the procedure was performed three times.[11]

Quantitative test for reducing sugars
Polysaccharide sulfate hydrolysate samples were prepared in two different volumes, namely 0.5 mL and 1 mL. A series of D-galactose standard solutions (0.2, 0.5, 1.0, 2.0, 5.0, and 10.0 mg/mL) were also prepared. Each hydrolysate sample and D-galactose standard solution were mixed with Benedict reagent and heated by boiling to ensure that the reaction was complete. All mixtures were cooled and centrifuged at 6000 rpm for 15 minutes to separate the copper oxide precipitate formed. The absorbance of the supernatant from each sample and standard was measured using a UV-Vis Spectrophotometer (Thermo Scientific, Waltham, USA) at a wavelength of 620 nm, to determine the concentration of reducing sugars in the hydrolysate samples based on the standard curve generated from the D-galactose solution. The procedure was performed three times.[11]

Preparation of ligands
The 2D structures of 3,6-Anhydro-D-galactose (3,6-D-AHG) and D-galactose were obtained from the PubChem database (Table 1). Both compounds were hydrolysis products of sulfated polysaccharides. The SMILES format was used as input for bioactivity and ADMET predictions. In general, SMILES (Simplified Molecular Input Line Entry System) is a linear notation system used to describe the structure of chemical molecules using short strings of ASCII characters.[12]

Table 1: Chemical information of tested compounds

No.	Compound Name	Molecular Formula	Molecular weight (g/mol)	SMILES & Source
1	3,6-Anhydro-D-galactose	$C_6H_{10}O_5$	162.14	C1[C@H]([C@@H]([C@H](O1) [C@H](C=O)O)O)O (https://pubchem.ncbi.nlm.nih.gov)
2	D-galactose	$C_6H_{12}O_6$	180.16	C([C@@H]1[C@@H]([C@@H]([C@H](C(O1)O)O) O)O)O (https://pubchem.ncbi.nlm.nih.gov)

Prediction of ligands' pharmacokinetic and toxicity properties
ADMETLab 2.0 is an integrated online platform used to predict absorption, distribution, metabolism, excretion, and toxicity properties of a chemical compound. The platform (https://admetmesh.scbdd.com/service/screening/molecule) was developed to assist in evaluating the potential of a compound as a drug candidate. It can predict 17 physicochemical properties, 13 medicinal properties, 23 ADME properties, 27 toxicity endpoints, and 8 toxicophor rules. ADMETLab 2.0 uses a QSPR (Quantitative Structure-Property Relationship) model trained with a multi-task graph attention (MGA) framework based on experimental ADMET data.[12]

Prediction of ligands' bioactivity
Bioactivity prediction of compounds from the Way2Drug PASS database was carried out based on the web server (https://www.way2drug.com/PASSOnline/) by entering SMILES data from 3,6-D-AHG and D-Galactose. The Pa (possibly active) and Pi (possibly inactive) values, ranging from 0 to 1, and generated by PASS Online, represent the biological activity of a compound based on the chemical structure. Compounds with a Pa value ≥ 0.7 are considered to have high biological activity potential, while those with a Pa value between 0.3 and 0.7 have moderate potential.[13]

Prediction of ligands' protein targets based on SMILES
The potential protein targets from SMILES of active compounds 3,6-anhydro-D-galactose and D-galactose were inputed into three different target prediction web server platforms, namely SwissTargetPrediction (http://www.swisstargetprediction.ch/), Similarity Ensemble Approach (SEA) (https://sea.bkslab.org/), and Super-PRED (https://prediction.charite.de/). Each of these platforms uses various algorithms and databases to predict which proteins in the human body will interact with the test compound based on structural similarity, pharmacophore, or other predictive models.[14,15]

Prediction of breast cancer protein targets
A comprehensive search was carried out, coupled with the collection of data from three major biomedical databases, namely Genecard at https://www.genecards.org/, Opentarget at https://www.opentargets.org/, and Disgenet at https://www.disgenet.org/. These databases aggregate information from a variety of literature sources, experimental data, and genetic studies to provide a list of genes and proteins associated with breast cancer pathogenesis, progression, or biomarkers.[16]

Assessment of pharmacology network
Pharmacology network was assessed by identifying overlapping protein targets between the predicted compound target and breast cancer-related protein target results. Cytoscape software was used to construct, visualize, and analyze this interaction network. Protein-protein interaction data in the network were enriched and validated using information from the STRING (Search Tool for the Retrieval of Interacting Genes/Proteins) database, which allows the identification of hub or central proteins that play key roles.[17]

Gene expression analysis
Gene expression of selected target proteins was analyzed using GEPIA2 (http://gepia2.cancer-pku.cn), an online platform based on RNA-seq data from Cancer Genome Atlas (TCGA) and Genotype-Tissue Expression (GTEx) projects. The "Expression DIY" feature was applied to compare the differential expression of target genes between breast cancer (BRCA) and normal tissues, followed by survival analysis.[18,19]

Molecular docking
Molecular docking was conducted to evaluate the interactions between the test ligand, 3,6-anhydro-D-galactose (3,6-D-AHG), and selected target proteins identified as the most promising candidates. The ligand structure was retrieved from PubChem and energy-minimized using the Open Babel function in PyRx (v0.8, The Scripps Research Institute, La Jolla, CA, USA). Protein structures were obtained from the Protein Data Bank (PDB) and prepared in PyMOL (Schrödinger, LLC, New York, USA) by removing water molecules and adding hydrogen atoms. Binding sites were predicted using PrankWeb, and docking was performed in PyRx, integrating AutoDock Vina (v1.2.0) with an exhaustiveness value of 8 and grid boxes covering the predicted sites. The most favorable docking pose was selected based on the lowest

ISSN 2616-0684 (Print)
ISSN 2616-0692 (Electronic)

binding energy, and interactions were analyzed using BIOVIA Discovery Studio (Dassault Systèmes, Vélizy-Villacoublay, France).[17,20] The overall *in silico* evaluation workflow is shown in Figure 1.

Redocking experiment

A docking validation was performed to assess the suitability of molecular docking protocol for the selected target proteins. As no co-crystallized ligand structures were available in the PDB, validation used the primary test ligand, 3,6-D-AHG, along with comparative ligands, including D-glucose and D-galactose (structural analogs), acetazolamide (a known inhibitor of carbonic anhydrase 12 (CA12)), and lonidamine (a known inhibitor of hexokinase 2).

Results and Discussion

FTIR spectral data of sulfated polysaccharides (Carrageenan)

The FTIR spectrum of the *ED sulfated polysaccharide extract* before hydrolysis showed a series of characteristic absorption bands, indicating the polysaccharide structure of carrageenan. A broad and very intense absorption band at a wavenumber of around 3446.79 cm^{-1} indicate the stretching vibrations of the hydroxyl (OH) groups of the polysaccharide sugar units and a large amount of bound water. The absorption at 2928.23 cm^{-1} corresponded to the C-H stretching vibrations of the aliphatic groups in the sugar ring. The presence of sulfate ester groups (SO_3^-), a major feature of carrageenan, was confirmed by a strong absorption band at 1257.59 cm^{-1}, which is characteristic of the asymmetric stretching vibration of S=O. The carbohydrate fingerprint region, which shows the C-O and C-O-C stretching vibrations of the glycosidic bonds and the pyranose ring, appeared dominant with a series of strong bands between 1035 cm^{-1} and 1157 cm^{-1}, specifically at 1070.49 cm^{-1} and 1035.77 cm^{-1} (Figure 2).

In a study of polysaccharides extracted from the red algae *Tichocarpus crinitus* and *Ahnfeltiopsis flabelliformis*, a typical absorption band was found at 932 cm^{-1}, showing the presence of the C–O group of 3,6-D-AHG, as well as bands at 849 cm^{-1} and 805 cm^{-1}, suggesting the presence of sulfate groups at C4 of galactose and C2 of 3,6-AHG, respectively. These results structurally confirmed the identity of the sulfated polysaccharides as κ/*β*-carrageenan and ι/κ-carrageenan types.[21] The combination of bands at 1257 cm^{-1}, 848 cm^{-1}, 802 cm^{-1}, and 927 cm^{-1} shows that the sulfated polysaccharide extract of ED is iota-carrageenan containing bioactive molecular compounds such as 3,6-D-AHG.

The FTIR spectrum for the polysaccharide sulfate hydrolysate showed a broad and strong band at a wavenumber of around 3427.51 cm^{-1} attributed to the stretching vibration of the OH group of the hydrolyzed sugar units and the bound water molecules (Figure 2). The absorption at 2926.01 cm^{-1} indicate the presence of aliphatic CH stretching vibration of the pyranose ring. One of the absorption bands typical of 3,6-D-AHG appeared in the region around 930 cm^{-1}, such as 883 $cm^{-1}$and 854 cm^{-1}, associated with the C–O group vibration on the anhydrous ring from 3,6-AHG. This band often indicates the existence of an anhydrous bridge between carbon 3 and 6 of galactose.[22,23] The absorption around 1070 cm^{-1} corresponded to C–O glycosidic group of 3,6-AHG bound to position 4 of the D-galactose unit.[22,24] Furthermore, the peak at 1707.00 cm^{-1} showed the presence of a carbonyl group, possibly from a terminal oxidation product formed during the hydrolysis process. In general, this spectrum shows a typical chemical profile of sulfated oligosaccharides, specifically those containing 3,6-D-AHG.

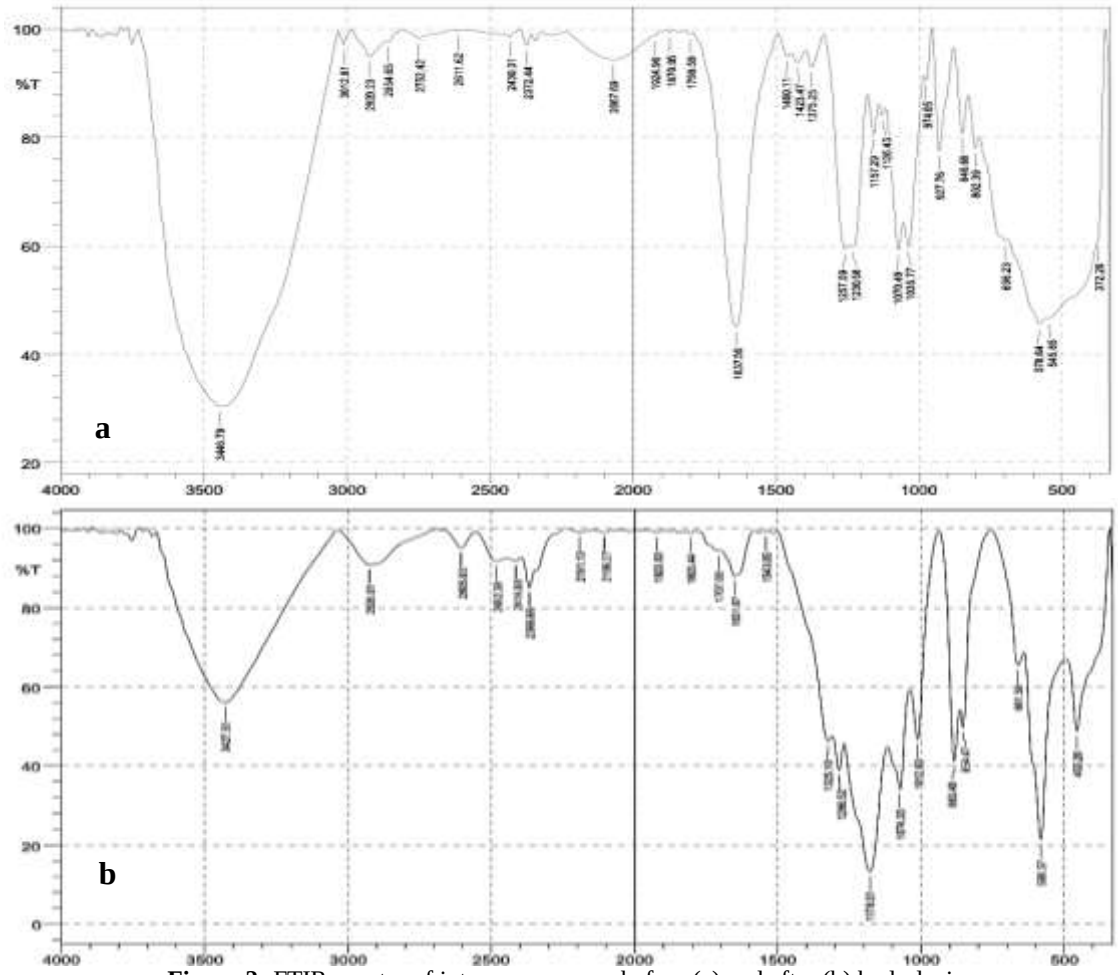

Figure 2: FTIR spectra of iota-carrageenan, before (a) and after (b) hydrolysis.

ISSN 2616-0684 (Print)
ISSN 2616-0692 (Electronic)

Sugar content of sulfated polysaccharide hydrolysate

The qualitative analysis using Benedict reagent showed a distinct colour change to reddish-brown, confirming the presence of reducing sugars in the sulfated polysaccharide hydrolysate from ED. This indicates that the reducing sugars reduced the blue Cu^{2+} ions from Benedict reagent to Cu^{+} ions, resulting in the formation of a coloured copper(I) oxide (Cu_2O) precipitate.

For the quantitative analysis, the sugar concentration was determined using a standard curve (y = 0.0049x – 0.002, R^2 = 0.9688) of D-galactose. At a sample volume of 0.5 mL, the absorbance values were 0.091 and 0.086, corresponding to sugar concentrations of 18.97 mg/mL and 17.69 mg/mL, respectively. These findings demonstrate that the hydrolysate contains a substantial level of reducing sugars, expressed as D-galactose equivalents.

The results, both qualitative and quantitative, confirmed the presence of reducing sugars in the sulfated polysaccharide hydrolysate, with concentrations showing a substantial amount of D-galactose equivalents. Similarly, previous studies reported that ED hydrolysates are rich in 3,6-anhydro-D-galactose, a monomer unit of κ-carrageenan known for potential bioactive properties.[9]

ADMET properties of test ligand

The compound 3,6-D-AHG met Lipinski criteria, showing a good potential ADMET profile. This compound has molecular weight (MW) < 500, LogP < 5, the number of hydrogen bond acceptors (nHA) < 10, and the number of hydrogen bond donors (nHD) < 5. The compound also met the rules of Pfizer and GSK,[25] showing a low probability of toxicity and a good pharmacokinetic profile (Table 2). The analysis also showed that the compound has a high MDCK permeability, indicating good absorption ability. In addition, the potential for hepatotoxicity (H-HT) is relatively low. In general, the results suggest that 3,6-Anhydro-D-galactose has desirable properties for further development as a drug candidate. Meanwhile, D-Galactose shows a promising profile as a drug candidate with good physicochemical properties, evidenced by the acceptance based on Lipinski and Pfizer rules, as well as hydrogen bond acceptors (nHA = 6) and donors (nHD = 5) in the optimal range. In terms of safety, D-Galactose showed a very low risk of liver toxicity, with H-HT values (0.041) in the "excellent" category. However, the MDCK permeability value of 3.0 $\times 10^{-7}$ cm/s showed low permeability, which needs to be considered in further development related to the absorption.

Table 2: ADMET properties of test compounds

No	Bioactive Compound	PubChem CID	Lipinski Rule	Pfizer Rule	nHA	nHD	H-HT	MDCK (cm/s)
1	3,6-Anhydro-D-galactose	16069996	Accepted	Accepted	5	3	0.088	0.000590527
2	D-Galactose	6036	Accepted	Accepted	6	5	0.041	0.000300731

Lipinski rule: logP ≤ 5, Hacc ≤ 10, Hdon ≤ 5, MW ≤ 500. A single violation is acceptable; ≥2 violations may result in poor permeability or absorption.
MW (Molecular weight): Optimal range is 100 - 600 Da, according to the Drug-Like Soft rule.
nHA (Hydrogen bond acceptors): Ideal range is 0 - 12, according to the Drug-Like Soft rule.
nHD (Hydrogen bond donors): Ideal range is 0 - 7, according to the Drug-Like Soft rule.
H-HT (Human intestinal absorption): Expressed as predictive value.
MDCK (Madin–Darby Canine Kidney permeability): Indicates membrane permeability. Results interpretation: The unit of predicted MDCK permeability is cm/s. A compound is considered to have a high passive MDCK permeability for a Papp > 20 x 10^{-6} cm/s, medium permeability for 2 - 20 x 10^{-6} cm/s, and low permeability for < 2 x 10^{-6} cm/s. Empirical decision: >2 x 10^{-6} cm/s: excellent (green), otherwise: poor (red).

Predicted bioactivity of test ligands

PASS analysis predicted that 3,6-D-AHG had a high probability of functioning as a glucose oxidase inhibitor (*Pa* = 0.871), NADPH peroxidase inhibitor (*Pa* = 0.837), and caspase-3 stimulant (*Pa* = 0.623) (Table 3). Compared to D-galactose, 3,6-D-AHG showed higher *Pa* scores in four out of five evaluated activities, suggesting a stronger potential to induce apoptosis and disrupt oxidative stress balance in cancer cells. Caspase-3 activation is a key execution step in apoptosis, while TP53 expression enhancement could restore tumor suppressor function. Furthermore, inhibiting oxidative stress–regulating enzymes such as NADPH peroxidase may selectively increase ROS in tumor cells, promoting apoptotic death (Figure 3).

Table 3: Prediction of compound bioactivity

No	Bioactive compound	Prediction Activity Score (Pa)					Relative bioactivity score
		Glucose oxidase inhibitor	NADPH peroxidase inhibitor	Chymosin inhibitor	TP53 Expression enhancer	Caspase-3 stimulant	
1	3,6-Anhydro-D-galactose	0.871	0.837	0.792	0.665	0.623	0.758
2	D-Galactose	0.809	0.728	0.736	0.765	0.737	0.760

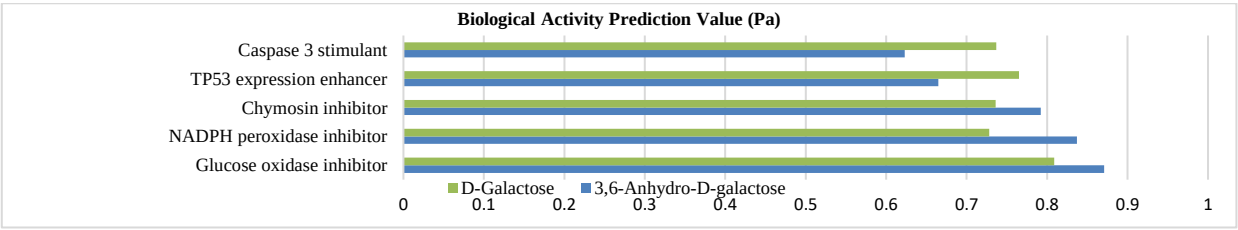

Figure 3: Predicted Values of Biological Activity (Pa) of 3,6-D-AHG and D-Galactose

ISSN 2616-0684 (Print)
ISSN 2616-0692 (Electronic)

Based on the results, 3,6-Anhydro-D-galactose (D-AHG) shows higher predicted biological activity than D-galactose in five key functions, namely caspase-3 stimulation, TP53 expression enhancement, and inhibition of chymosin, NADPH peroxidase, and glucose oxidase. As a caspase-3 stimulant, D-AHG plays a critical role in activating apoptosis pathways, leading to cancer cell destruction.[26] The predicted ability to enhance TP53 expression, a major tumor suppressor, supports cell growth control and apoptosis induction. Chymosin inhibition suggests potential suppression of cancer cell invasion and metastasis. D-AHG also inhibits NADPH peroxidase, disrupting redox balance, elevating ROS levels, and triggering apoptosis, as well as glucose oxidase, which elevates intracellular hydrogen peroxide and generates hydroxyl radicals, enhancing oxidative damage and apoptosis in breast cancer cells.[23] Additionally, glucose oxidase inhibition may impair cancer cell energy supply by increasing glucose consumption. These results provide an initial pharmacological profile supporting the potential of D-AHG and D-galactose as anticancer agents through apoptosis induction and oxidative stress modulation.[30]

Predicted protein target based on SMILES

The protein target prediction data from both compounds show the potential for interaction with various protein targets. The compound 3,6-D-AHG was predicted to have a high probability of interaction score with targets such as DNA-(apurinic or apyrimidinic site) lyase (APEX1) (91.22%) and Endoplasmic Reticulum-associated Amyloid b-peptide-bp (HSD17B10) (93.68%) according to SUPER Target. SEA Target produced the highest score on YARSI (Tyrosine--tRNA ligase, cytoplasmic) with 1.965277778, and SWISST Target showed a value of 0.0439186325197 for several targets, including GBA and FOLH1. Meanwhile, D-Galactose showed potential interactions with several types of galectins (LGALS3, LGALS4, LGALS8) and Carbonic anhydrase (CA1, CA9, CA12) according to SEA Target, as well as Bloom syndrome protein (BLM) (95.81%) based on SUPER Target (Table 4).

Table 4: Predicted protein targets of 3,6-D-AHG

Target name	Target common name	Data Source	Probability or MaxTc*
YARS1	Tyrosine--tRNA ligase, cytoplasmic	SEA Target	1.965277778
GBA	Beta-glucocerebrosidase	SWISS Target	0.0439186325197
FOLH1	Glutamate carboxypeptidase II	SWISS Target	0.0439186325197
PRKCA	Protein kinase C alpha	SWISS Target	0.0439186325197
PRKCD	Protein kinase C delta (by homology)	SWISS Target	0.0439186325197
CA2	Carbonic anhydrase II	SWISS Target	0.0439186325197
CA12	Carbonic anhydrase XII	SWISS Target	0.0439186325197
TRIM24	Transcription intermediate factor 1-alpha	SUPER Target	80.23%
PIK3CB	PI3-kinase p110-beta subunit	SUPER Target	80.5%
GLRA1	Glycine receptor alpha-1 subunit	SUPER Target	83.54%
TOP2A	DNA topoisomerase II alpha	SUPER Target	83.86%
CNR2	Cannabinoid CB2 receptor	SUPER Target	84.17%
NFKB1	Nuclear factor NF-kappa-B p105 subunit	SUPER Target	86.01%
ALOX12	Arachidonate 12-lipoxygenase	SUPER Target	86.59%
APEX1	DNA-(apurinic or apyrimidinic site) lyase	SUPER Target	91.22%
HSD17B10	Endoplasmic reticulum-associated amyloid b-peptide-bp	SUPER Target	93.68%

*Each database source has a different probability format or unit or standard.

Hexokinase 2 (HK2), one of the targets of D-galactose, is a key isoform in the hexokinase family of enzymes and plays a role in the initiation of glycolysis, namely, phosphorylation of glucose into glucose-6-phosphate. In the context of cancer, HK2 contributes to the metabolism of cell glycolysis-dependent cancer aerobes, a phenomenon known as the Warburg effect.[31,32] The ability of compounds such as D-galactose or derivatives to interact with or inhibit HK2 provides opportunities for promising therapeutics. Five overlapping target proteins were identified between the two compounds, while 3,6-D-AHG had 11 specific protein targets, D-galactose had 42 specific protein targets (Table 5). The five overlapping proteins with significant potential to be common targets of the two compounds are GBA (beta-glucocerebrosidase), CA12 (carbonic anhydrase XII), NFKB1 (nuclear factor NF-kappa-B p105 subunit), APEX1 (DNA-(apurinic or apyrimidinic site) lyase), and HSD17B10 (endoplasmic reticulum-associated amyloid beta-peptide-binding protein). The function of each of these proteins, such as the role of GBA in lipid metabolism, CA12 in pH regulation, NFKB1 in inflammation and immunity, and APEX1 in DNA repair, suggests diverse biological pathways simultaneously affected by the two compounds.

Table 5: Predicted protein targets of D-Galactose

Target name	Target common name	Data Source	Probability or MaxTc*
OGA	O-GlcNAcase Protein	SEA Target	2.655555556
FGF2	Fibroblast growth factor 2	SEA Target	2.540972222
GJB2	Gap junction beta-2 protein	SEA Target	2.371527778
LGALS4	Galectin-4	SEA Target	2.670833333
LGALS8	Galectin-8	SEA Target	2.670833333
ADK	Adenosine kinase	SEA Target	2.149305556

ISSN 2616-0684 (Print)
ISSN 2616-0692 (Electronic)

UMPS	Uridine 5'-monophosphate synthase	SEA Target	2.202083333
VEGFA	Vascular endothelial growth factor A	SEA Target	2.540972222
ERAP1	Endoplasmic reticulum aminopeptidase 1	SEA Target	2.160416667
LGALS3	Galectin-3	SEA Target	2.670833333
CA1	Carbonic anhydrase 1	SEA Target	3.472222222
IL6	Interleukin-6	SEA Target	1.9625
HSPA5	Endoplasmic reticulum chaperone BiP	SEA Target	2.052083333
SLC5A1	Sodium/glucose cotransporter 1	SEA Target	2.209722222
CA9	Carbonic anhydrase 9	SEA Target	3.472222222
SLC5A4	Solute carrier family 5 members 4	SEA Target	2.113194444
PDCD4	Programmed cell death protein 4	SEA Target	2.099305556
CA12	Carbonic anhydrase 12	SEA Target	3.472222222
AGL	Glycogen debranching enzyme	SEA Target	2.025694444
GLB1	Beta-galactosidase	SEA Target	3.086111111
PYGMY	Glycogen phosphorylase, muscle form	SEA Target	2.430555556
MGAM	Maltase-glucoamylase, intestinal	SEA Target	2.314583333
HK1	Hexokinase-1	SEA Target	2.479861111
HK2	Hexokinase-2	SEA Target	2.479861111
GLA	Alpha-galactosidase A	SEA Target	2.314583333
THERE IS	Adenosine deaminase	SEA Target	2.371527778
AMY2A	Pancreatic alpha-amylase	SEA Target	2.314583333
HEXA	Beta-hexosaminidase alpha subunit	SEA Target	2.655555556
CD69	Early activation antigen CD69	SEA Target	2.264583333
TYR	Tyrosinase	SEA Target	2.261111111
FGF1	Fibroblast growth factor 1	SEA Target	2.540972222
HEXB	Beta-hexosaminidase beta subunit	SEA Target	2.655555556
SLC5A2	Sodium/glucose cotransporter 2	SEA Target	2.700694444
GANC	Neutral alpha-glucosidase C	SEA Target	2.314583333
PYGB	Glycogen phosphorylase, brain form	SEA Target	2.122222222
CDA	Cytidine deaminase	SEA Target	2.507638889
GBA	Beta-glucocerebrosidase	SWISS Target	0.141787380829
HSP90AA1	Heat shock protein HSP 90-alpha	SWISS Target	0.133391037839
VEGFA	Vascular endothelial growth factor A	SWISS Target	0.133391037839
PSEN2 PSENEN NCSTN APH1A PSEN1 APH1B	Gamma Secretase	SWISS Target	0.133391037839
FGF1	Acidic fibroblast growth factor	SWISS Target	0.133391037839
FGF2	Basic fibroblast growth factor	SWISS Target	0.133391037839
HPSE	Heparanase	SWISS Target	0.133391037839
CDK1	Cyclin-dependent kinase 1	SWISS Target	0.125075959828
LGALS4	Galectin-4	SWISS Target	0.125075959828
LGALS3	Galectin-3	SWISS Target	0.125075959828
LGALS8	Galectin-8	SWISS Target	0.125075959828
PYGB	Brain glycogen phosphorylase	SWISS Target	0.116739032206
TDP1	Tyrosyl-DNA phosphodiesterase 1	SUPER Target	83.31%
APEX1	DNA-(apurinic or apyrimidinic site) lyase	SUPER Target	87.25%

ISSN 2616-0684 (Print)
ISSN 2616-0692 (Electronic)

NFKB1	Nuclear factor NF-kappa-B p105 subunit	SUPER Target	87.29%
ADK	Adenosine kinase	SUPER Target	88.61%
HSD17B10	Endoplasmic reticulum-associated amyloid beta-peptide-binding protein	SUPER Target	90.77%
ADORA1	Adenosine A1 receptor	SUPER Target	91.94%
NOT YET	Bloom syndrome protein	SUPER Target	95.81%

*Each database source has a different probability format or unit or standard.

Predicted breast cancer protein targets

Breast cancer is a multifactorial disease characterized by genetic and epigenetic alterations in various molecular pathways. Bioinformatics analysis from various sources such as DisGeNET, Open Targets, and GeneCards showed more than 900 potential protein targets associated with breast cancer, including important ones such as BRCA1, BRCA2, TP53, PIK3CA, ERBB2 (HER2), and ESR1 (Figure 4). From these databases, 20 protein targets were found to overlap with D-galactose and 3,6-Anhydro-D-galactose (3,6-D-AHG), suggesting significant potential for breast cancer treatment. D-galactose was predicted to target proteins ADKP3:Q25, VEGFA, IL6, HSPA5, PDCD4, GLB1, HK1, GLA, ADA, TYR, HEXB, HSP90AA1, CDK1, APEX1, NFKB1, and BLM. These proteins play a role in the angiogenesis pathway (VEGFA), inflammation (IL6, NFKB1), cellular stress (HSPA5, HSP90AA1), cell cycle (CDK1), and DNA repair (APEX1, BLM).[32] Meanwhile, 3,6-D-AHG was predicted to target proteins PRKCA, PRKCD, CA2, PIK3CB, TOP2A, NFKB1, and APEX1, which play a role in transduction signal proliferation (PIK3CB, PRKCA), cell metabolism (CA2), as well as DNA synthesis and repair processes (TOP2A, APEX1)[33] (Figure 4).

The Venn diagram analysis of target protein for D-galactose (Figure 5a) and 3,6-Anhydro-D-galactose (3,6-D-AHG) (Figure 5b) against cancer target protein cluster from three bioinformatics databases, namely; GeneCards (GC), Open Targets (OT), and DisGeNET (DG) shows significant overlaps. From over 100 cancer targets identified, 16 proteins overlapped directly with D-Galactose, while 7 proteins overlapped with 3,6-D-AHG. D-Galactose was predicted to interact with VEGFA, IL6, HSPA5, CDK1, APEX1, and NFKB1, which play a role in angiogenesis, inflammation, cell cycle, and DNA repair. On the other hand, 3,6-D-AHG interacted with PRKCA, PIK3CB, TOP2A, APEX1, and NFKB1, which are generally associated with signal proliferation and stress response. These results suggest that both compounds may exert anticancer effects through the modulation of key molecular proteins in the development of breast cancer.

Pharmacology network

Pharmacological network analysis was carried out to examine target proteins of D-galactose and 3,6-Anhydro-α-D-galactose (3,6-D-AHG) compounds previously mapped against hundreds of breast cancer targets from DisGeNET, Open Targets, and GeneCards databases. The results showed that several proteins have central roles in the interaction network, including IL6, NFKB1, HSP90AA1, CDK1, and TOP2A (Figure 6). The highest *betweenness centrality* and *closeness centrality values* were found in IL6 and HSP90AA1, showing their central roles in important functional pathways such as inflammation, cellular stress, and drug resistance. NFKB1 and APEX1 were found as the target intersections of D-galactose and 3,6-D-AHG, showing the potential modulation of inflammation and DNA repair, two crucial pathways in breast cancer development and survival. Furthermore, the compound 3,6-D-AHG was shown to specifically target HSPA5 with *a degree value of* 5 (eighth order) and *a closeness centrality value* of 0.514285714 (Table 6). HSPA5 plays a role in the response to endoplasmic reticulum stress, as well as regulating apoptosis. This protein, also known as GRP78, is a marker of reticulum stress often overexpressed in cancer cells and associated with poor prognosis and resistance to therapy.[34]

Based on the entire process, starting from the initial identification of predicted protein targets to the analysis of interactions in biological networks, four key proteins were further assessed in molecular docking stage, namely; CA12 (Carbonic Anhydrase XII), Galectin-3 (LGALS3), Hexokinase-2 (HK2), and HSPA5 (Heat Shock Protein Family A Member 5). The selection of these proteins was based on the functional significance and potential as therapeutic targets. Although HK2, CA12, and LGALS3 did not appear in the analysis of network centrality, such as IL6, NFKB1, or TOP2A, the existence remains important. This is because their function as regulators of metabolism supports energy proliferation in cancer cells and is included in the prediction of target proteins based on compounds studied (Tables 3 and 4).

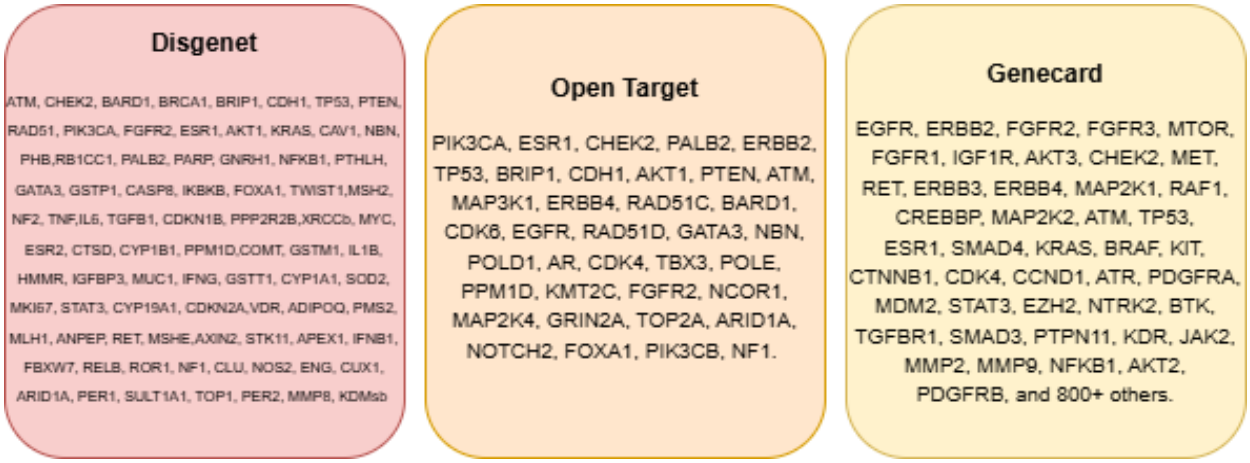

Figure 4: List of target protein collections based on breast cancer disease from the Genecard (GC), Open Target (OT), and Disgenet databases

ISSN 2616-0684 (Print)
ISSN 2616-0692 (Electronic)

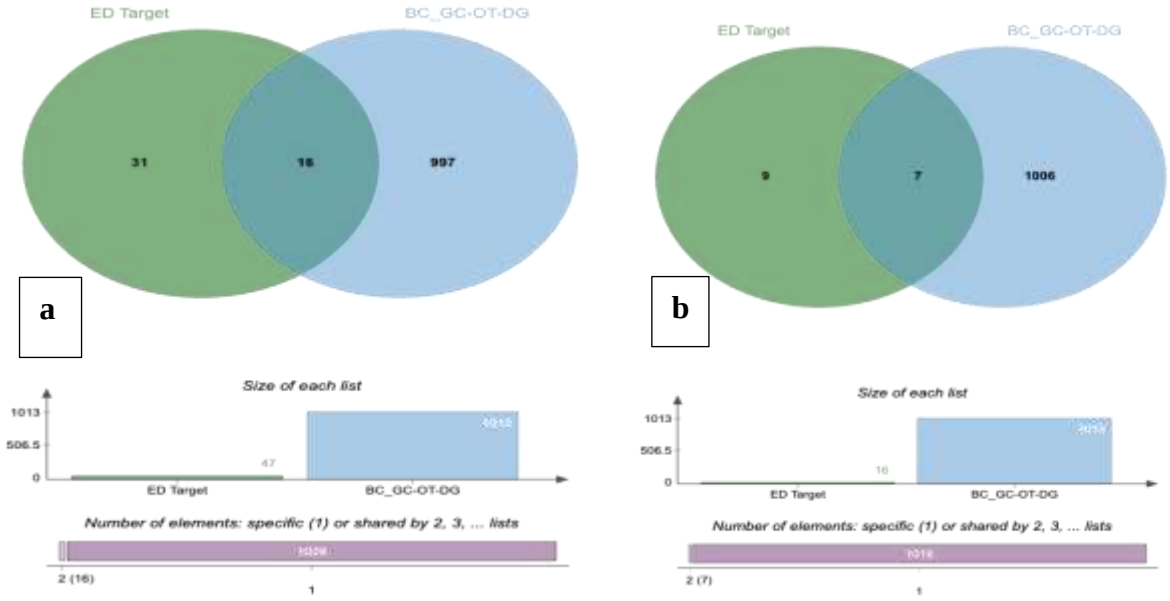

Figure 5: Overlapping Venn diagram of protein targets between D-Galactose with Genecard (GC), Open Target (OT), and Disgenet database sources (a) and 3,6-D-AHG with the same three database sources (b)

Table 6: Interactions between target proteins

No	Name	Betweenness Centrality	Closeness Centrality	Degree	Average Shortest Path Length	Neighborhood Connectivity
1	IL6	0.429084967	0.620689655	9	1.611111111	4.111111111
2	HSP90AA1	0.362309368	0.620689655	8	1.611111111	5.125
3	NFKB1	0.097494553	0.5625	7	1.777777778	5.285714286
4	CDK1	0.079956427	0.514285714	5	1.944444444	6.4
5	TOP2A	0.036928105	0.45	5	2.222222222	4.6
6	PRKCD	0.043464052	0.5	5	2	6
7	PRKCA	0.020043573	0.461538462	4	2.166666667	6.5
8	HSPA5	0.11546841	0.514285714	4	1.944444444	6.5
9	GLB1	0.016339869	0.333333333	3	3	2.333333333
10	GLA	0.162309368	0.43902439	3	2.277777778	4.333333333

Gene expression analysis data

Gene expression analysis with the GEPIA2 platform was used to compare mRNA expression for the four main target genes, namely; CA12, LGALS3, HK2, and HSPA5, in breast cancer tissue (BRCA) to the normal breasts. Data were collected from TCGA and GTEx projects, with samples of 1,085 (tumor) and 291 (normal), respectively. The results showed that the CA12 gene was more expressed than other genes in breast cancer network compared to normal ($p < 0.05$), as shown by the clear difference in median log2(TPM+1) expression in the box plot (Figure 7a). Elevated expression of CA12 has been reported to correlate with a more aggressive breast cancer subtype, specifically hormone receptor-positive tumors.[35] In contrast, the expression of LGALS3, HK2, and HSPA5 genes did not show significant differences between breast cancer and normal tissue (Figures 7b, 7c, and 7d).

CA12 is known to play a role in maintaining intracellular pH homeostasis and the tumor microenvironment, facilitating the adaptation of cancer cells to hypoxia and acidic conditions.[35] HK2, a key enzyme in glycolysis and often associated with the Warburg effect, did not show significant overexpression in the BRCA network. This shows that HK2 regulation in breast cancer is complex, possibly comprising post-transcriptional or activation through a metabolic signaling pathway.[32] HSPA5 is frequently and highly expressed in breast cancer, specifically in triple-negative and HER2+ subtypes, both associated with poor prognosis.[36,37] However, the results of GEPIA2 analysis showed that HSPA5 expression did not differ significantly between cancer and normal tissues, reflecting post-transcriptional or subtype-specific regulation.[31] LGALS3 (Galectin-3), which plays a role in adhesion, migration, and apoptosis evasion, also did not show significantly increased expression in the GEPIA2 dataset. This protein remains relevant as a therapeutic target due to their role in tumor microenvironment regulation and resistance to hormonal therapy. Their expression is considered to better reflect post-translational regulatory dynamics, subcellular location, or protein-carbohydrate interactions at the cell surface, which are not directly reflected by RNA-seq data. Therefore, LGALS3 remains a viable target for therapeutic exploration, particularly through the approach of inhibiting galectin–ligand interactions using sugar-based small molecules.[38] The results strengthen the relevance of CA12, HK2, HSPA5, and LGALS3 as promising molecular targets for breast cancer.

ISSN 2616-0684 (Print)
ISSN 2616-0692 (Electronic)

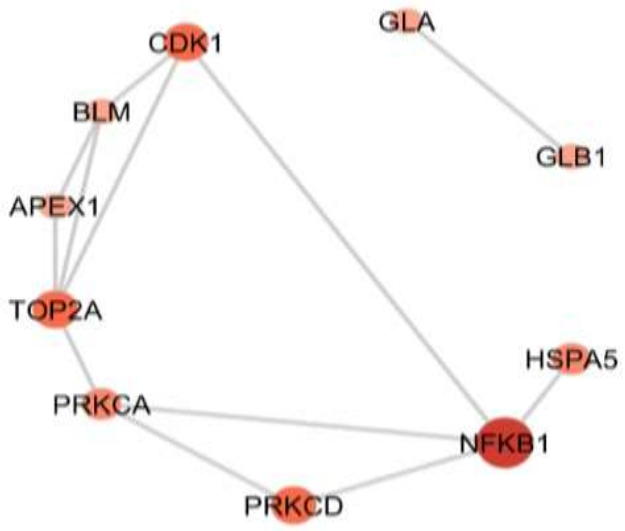

Figure 6: Illustration of Interaction between Target Proteins

Molecular docking results

The molecular docking results presented in Table 7 showed that the test ligand 3,6-D-AHG had a higher binding affinity (more negative energy value) compared to the natural control ligands (D-Galactose and D-Glucose) for the four main protein targets (HK2, CA12, HSPA5, LGALS3). The ligand 3,6 D-AHG showed the lowest binding affinity, and was predicted to have the most stable interaction with HK2 (GDP ID: 2NZT) and HSPA5 (GDP ID: 3IUC), as evidenced by an energy of -5.6 kcal/mol each. For the CA12 protein (PDB ID: 4HT2), D-glucose and 3.6 D-AHG showed similar and significantly strong binding affinity (-5.3 kcal/mol). Meanwhile, D-Galactose had the best interaction with Galectin-3 (PDB ID: 1KJL) as shown by an affinity of -4.6 kcal/mol.

Structurally, D-glucose is a simple monosaccharide very similar to D-galactose and 3,6-D-AHG, making it suitable as a negative control in molecular interaction study against cancer protein targets. The physiological role in cancer cell metabolism is also very relevant, considering that cancer cells have high glucose consumption through the Warburg effect.[40] Glucose is not only the main substrate of glycolysis, but also interacts with proteins such as hexokinase, glucose transporters (GLUTs), and several lectin-domain proteins, including Galectin-3, through the introduction of terminal hydroxyl groups. It plays a central role in supporting tumor cell growth and survival through increased uptake and activation of the PI3K-Akt pathway.[32] Therefore, evaluating the binding ability of D-glucose to targets such as HK2, HSPA5, or LGALS3 provides a biologically relevant molecular baseline to assess the structural and pharmacophoric performance of derivatives, including 3,6-D-AHG. As a neutral and physiological reference compound, D-glucose confirmed that the increased binding affinity of 3,6-D-AHG was not simply an effect of the basic sugar structure, but rather a result of specific chemical modifications, enhancing the interaction with the active site of the target protein (Figures 9 and 10).

Table 7: Molecular docking results of target proteins HK2, CA12, HSPA5 and LGALS3

Protein	Ligand	Binding Affinity (kcal/mol)	Conventional Hydrogen Bond	Van der Waals	Unfavorable donors–donors*
HK2 (ID: 2NZT, Chain: A)	D-Glucose	-4.6	GLY A:87, ILE A:114	LEU A:85, GLY A:86, THR A:88, PHE A:90, ASN A:89, TYR A:112, ALA A:113, PRO A:115, MET A:119, PHE A:175, THR A:232	-
	D-Galactose	-4.3	TYR A:112, GLY A:87, PHE A:90, THR A:88, ILE A:114	LEU A:85, ASN A:89, ALA A:113, MET A:119, PHE A:175	GLY A:86
	3.6 D-AHG	-5.6	ASN A:235, SER A:155, SER A:172, ASN A:208, LYS A:173, ASP A:209, GLY A:233, SER A:234	PHE A:156, PRO A:157, GLU A:260, GLY A:262, GLU A:294, GLN A:291, ILE A:229, THR A:210, THR A:232	-
	Lonidamine	-5.0	LYS A:176, SER A:178	GLY A:121. SER A:122, ARG A:120, VAL A:180, ARG A:183	SER: 178
CA12 (ID: 4HT2 Chain: D)	D-Galactose	-5.2	THR198, THR199, PRO200	-	HIS93
	D-Glucose	-5.3	THR199, GLN89, HIS93	-	-
	3.6 D-AHG	-5.3	THR198, THR199, GLN89, HIS91, HIS93	HIS91	HIS93
	Acetazolamide	-6.1	ASN D:96, ASN D:98, ASN D:244	PRO D:97, ILE D:243	-
	D-Glucose	-5	ASP A:224, ASP A:231, LYS A:96, ADP A:1, THR A:229	LEU A:35, LEU A:225, PRO A:173, GLU A:201, ASP A:34, VAL A:394, GLY A:226, GLY A:363, GLY A:36	THR A:229, THR A:37, CA A:411

HSPA5 (ID: 3IUC, Chain: A)	D-Galactose	-5	THR A:57, THR A:229, ASP A:201	PHE A:230, LEU A:225, GLY A:226, ASP A:224, GLY A:363, VAL A:394, ASP A:291, PRO A:173, GLY A:136, LEU A:95, GLU A:201	CA A:411, LYS A:96
	3.6 D-AHG	-5.6	THR A:37, ASP A:131	TYR A:39, ASP A:1, GLY A:36, LYS A:96, PRO A:173, THR A:229, GLU A:201, ASP A:224, GLY A:226, VAL A:394	CA A:411
LGALS3 ID: 1KJL, Chain: A	D-Glucose	-4.3	ASN143, ASN164, GLU165	ASN160, ASN166	ARG162, ASN143
	D-Galactose	-4.6	ASN164	ASN143, ASN160, ASN166, ARG144, GLU165, PHE163	ARG162
	3.6 D-AHG	-4.1	ARG162, ASN160, ASN174, HIS158	TRP181, VAL172, ARG144, GLU184	-

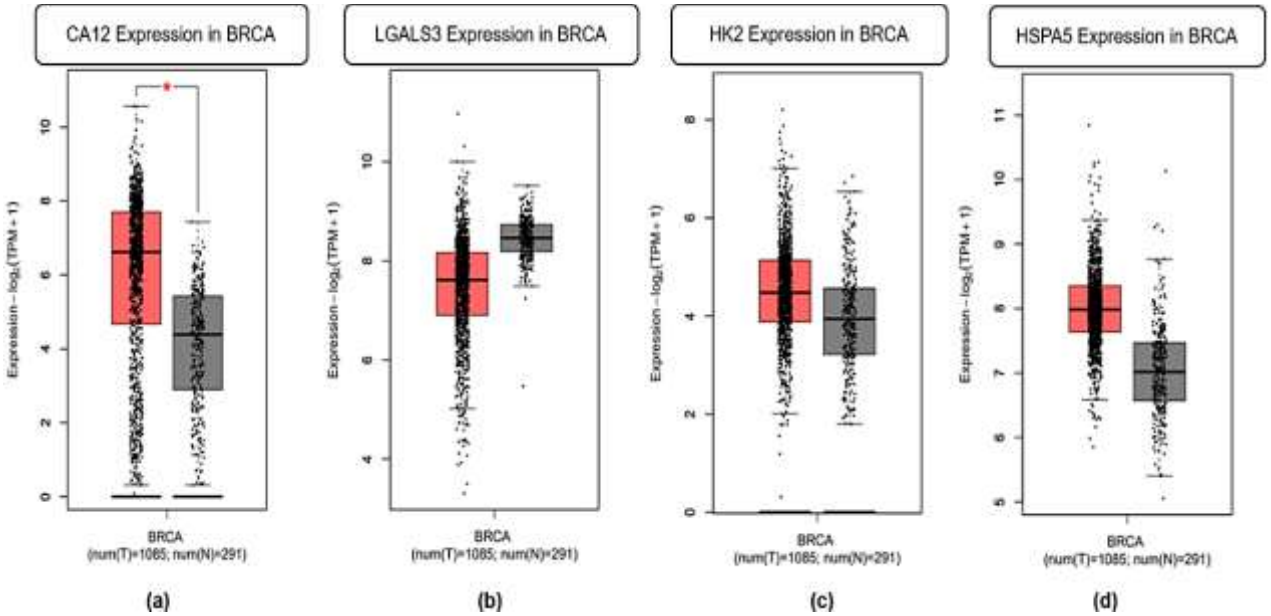

Figure 7: Expression profiles of target genes associated with breast cancer from GEPIA2 analysis: (a) CA12, (b) LGALS3, (c) HK2, and (d) HSPA5, showing significant differences between tumor (BRCA) and normal breast tissue

Docking results between D-Glucose and 3,6-D-AHG with target proteins showed differences in interaction patterns and contact densities. The ligand 3,6-D-AHG appeared to form a more extensive interaction network, specifically hydrogen bonds, with HK2 and HSPA5 proteins, which visually supports the stronger binding affinity data (-5.6 kcal/mol for 3,6-D-AHG with both proteins compared to -4.6 kcal/mol and -5 kcal/mol for D-Glucose with HK2 and HSPA5, respectively). In HK2, 3,6-D-AHG formed many conventional hydrogen bonds surrounding the ligand, while D-Glucose also formed hydrogen bonds, but with apparently different numbers and distributions. This was supported by the formation of specific hydrogen bond interactions between 3,6 D-AHG and ASN A:235, SER A:155, as well as significant Van der Waals interactions. However, several potential interactions with less favorable donors were also recorded in several complexes. In HSPA5, 3,6-D-AHG appeared to fit tightly in the binding pocket with some hydrogen bonds and significant Van der Waals interactions. For CA12, both ligands showed some hydrogen bonds, but 3,6-D-AHG also indicated Pi-donor hydrogen bond interactions, not observed in the D-Glucose complex. In Galectin-3, D-Glucose had some conventional hydrogen bonds (Figure 8), while 3,6-D-AHG, in addition to hydrogen bonds, also showed metal-acceptor interactions and some less favorable contacts, contributing to the slightly lower affinity compared to D-Galactose. Although D-Galactose was not visualized for direct comparison with 3,6-D-AHG here, the affinity of -4.1 kcal/mol ranked highest among all ligands for Galectin-3 (Figure 8), These visualizations (Figures 8 and 9) showed the structural differences between D-Glucose and 3,6-D-AHG, resulting in varying binding modes and types of interactions with amino acid residues in the active site of target proteins, which may affect the stability of the ligand-protein complex.

As positive controls, Acetazolamide was used for the CA12 target, and Lonidamine for the HK2 target (Table 7 and Figure 10). Acetazolamide stably binds to CA12 protein, mainly through two conventional hydrogen bonds with ASN residues D:96 and ASN D:244 strengthened by van der Waals contacts. Meanwhile, the lonidamine ligand showed a more diverse binding mode to HK2 protein, comprising a combination of hydrogen bonds to LYS A:176, Pi-Anion to GLU A:181, Pi-Sigma to TRP A:171, and extensive van der Waals interactions with

ISSN 2616-0684 (Print)
ISSN 2616-0692 (Electronic)

surrounding residues. Acetazolamide is a classical carbonic anhydrase inhibitor that has been used for targeting CA IX and CA XII in various cancers. It has shown specific inhibitor activity through interaction with the catalytic zinc sites. The compound showed the highest affinity, with important interactions at the catalytic site of Zn^{2+} ions and active residues such as HIS and THR. Lonidamine is an anticancer agent that has been used in combination chemotherapy and in clinical trials for the treatment of tumors refractory to conventional chemotherapy. It inhibits mitochondrial-bound HK2, disrupting the metabolism of glucose and producing a decrease in ATP and induction of apoptosis in cancer.[41] Based on the results, lonidamine showed the strongest binding affinity among all compounds with the lowest energy, supported by the interaction of extensive hydrophobicity and π-sulfur bonds at the active site of mitochondrial HK2 (Figure 10). However, 3,6-D-AHG is also capable of forming stable hydrogen and π interactions, despite lacking an aromatic group complex. This compound also formed a combination of hydrogen bonds and van der Waals forces, creating a sufficient complex interaction network. This suggests that despite the relatively simple structure, 3,6-D-AHG is potentially competitive compared to the positive ligands (Figure 9). The use of positive control is to evaluate whether the test compound is capable of approaching the binding activity of ligands previously validated through experimental or clinical studies. The results showed that 3,6-D-AHG has a binding affinity value close to the positive control, while also indicating complex interaction compared to D-glucose. This provides a strong basis for considering the simple structural modifications that could further improve selectivity against the target molecule (Figure 9).

Molecular docking results offer valuable preliminary insights into the potential of 3,6 D-AHG to inhibit or modulate the target protein by the test ligand. The more negative bond generally shows a more stable interaction and significant potential for further development of therapeutic agents. Analysis of the type and position of bond in the interaction of 3,6 D-AHG with THR A:37 and ASP A:131 in HSPA5 is very crucial in understanding the mechanism of interaction at molecular level and for future ligand optimization.

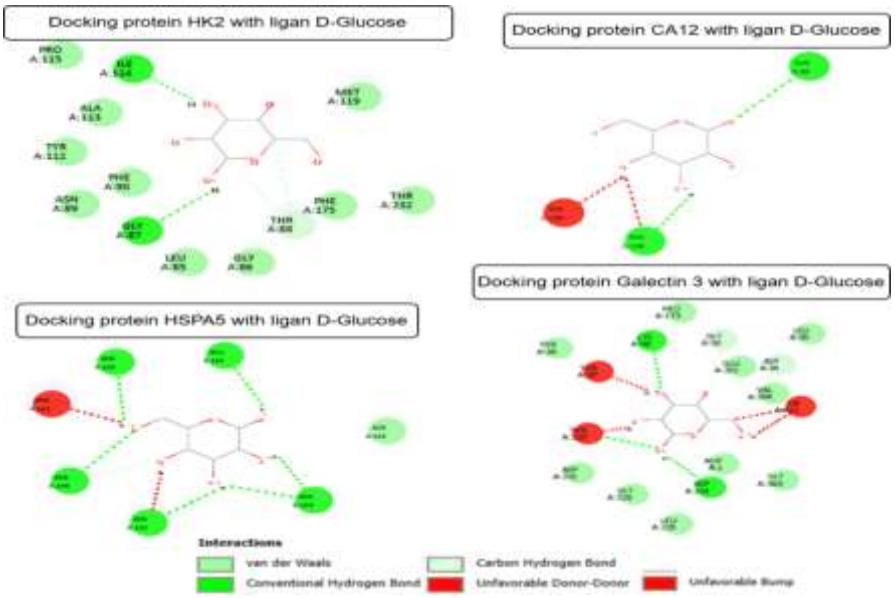

Figure 8: Visualization of docking interaction of four target proteins with D-Glucose

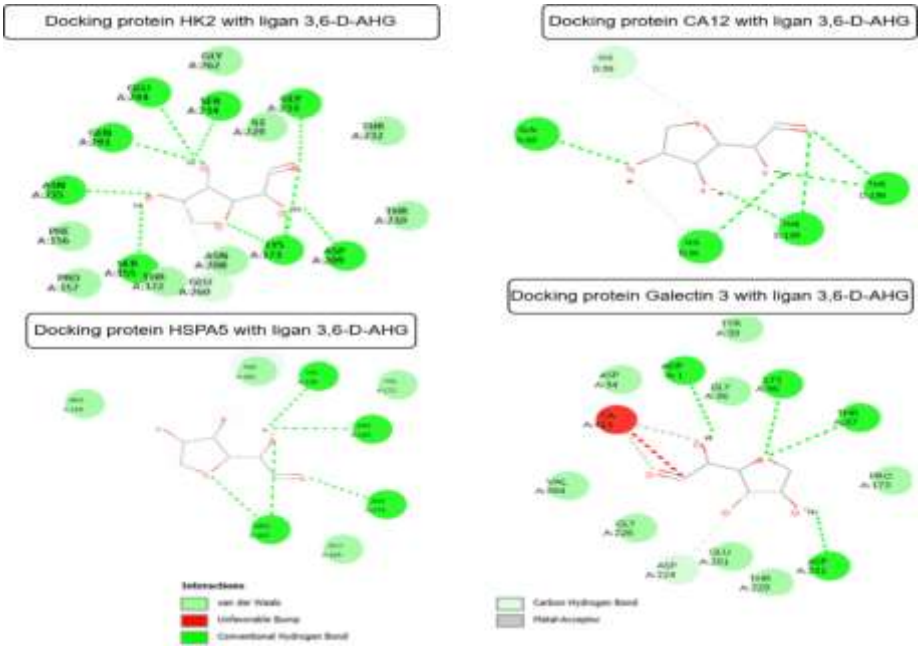

Figure 9: Visualization of docking interaction of four target proteins with 3,6-D-AHG

ISSN 2616-0684 (Print)
ISSN 2616-0692 (Electronic)

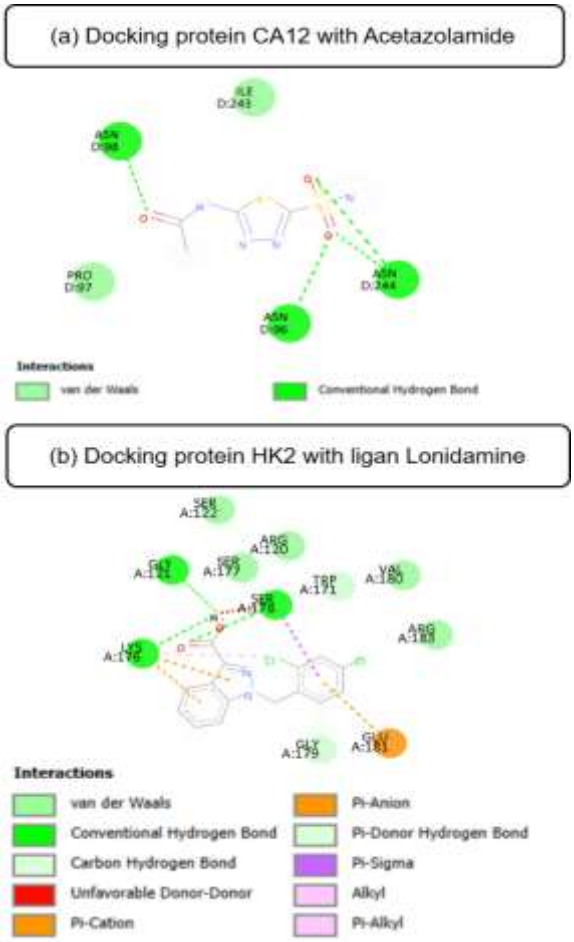

Figure 10: Visualization of docking interaction of CA12 (a) and HK2 (b) with positive control ligand

Conclusion

In conclusion, ED seaweed polysaccharide sulfate showed significant potential as an anti-breast cancer agent. This potential was supported by favorable pharmacokinetic predictions, low toxicity, and the ability of the hydrolytic product, 3,6-Anhydro-D-galactose (3,6-D-AHG), to modulate apoptosis through glucose oxidase inhibition. Key results include strong and stable molecular docking affinity of 3,6-D-AHG with key breast cancer-related proteins such as HK2 and HSPA5 (both at –5.6 kcal/mol), showing better binding than the natural control compound. These interactions suggest the compound's ability to disrupt cancer cell metabolism and stress response mechanisms. Although this study is predictive, the results provide a promising basis for further *in vitro* and *in vivo* validation to confirm 3,6-D-AHG potential as a novel anticancer agent from Indonesian marine bioresources.

Conflict of Interest

The authors declare no conflict of interest.

Authors' Declaration

The authors hereby declare that the work presented in this article is original and that any liability for claims relating to the content of this article will be borne by them.

Acknowledgements

The authors are grateful to the Graduate School of Hasanuddin University for the support in conducting the study.

References

1. Ferrari AJ, Santomauro DF, Aali A, Abate YH, Abbafati C, Abbastabar H, Abd ElHafeez S, Abdelmasseh M, Abd-Elsalam S, Abdollahi A, Abdullahi A, Abeldaño Zuñiga RA, Aboagye RG, Abolhassani H, Abreu LG, Abualruz H, Abu-Gharbieh E, Abu-Rmeileh NM, Murray CJL. Global Incidence, Prevalence, Years Lived with Disability (YLDs), Disability-Adjusted Life-Years (DALYs), and Healthy Life Expectancy (HALE) for 371 Diseases and Injuries in 204 Countries and Territories and 811 Subnational Locations, 1990–2021: A Systematic Analysis for the Global Burden of Disease Study 2021. Lancet. 2024; 403(10440):2133–2161.
2. Sung H, Ferlay J, Siegel RL, Laversanne M, Soerjomataram I, Jemal A, Bray F. Global Cancer Statistics 2020: GLOBOCAN Estimates of Incidence and Mortality Worldwide for 36 Cancers in 185 Countries. CA Cancer J Clin. 2021; 71(3):209–249.
3. International Agency for Research on Cancer (IARC). GLOBOCAN 2022: Indonesia – Fact Sheet: All Cancers [Internet]. World Health Organization; 2022 [cited 2025 Sep 15]. Available from: https://gco.iarc.fr/today/data/factsheets/populations/360-indonesia-fact-sheets.pdf.
4. Waks AG and Winer EP. Breast Cancer Treatment: A Review. JAMA. 2019; 321(3):288–300.
5. Necas J and Bartosikova L. Carrageenan: A Review. Vet Med (Praha). 2013; 58(4):187–205.
6. Bayu A, Warsito MF, Putra MY, Karnjanakom S, Guan G. Macroalgae-Derived Rare Sugars: Applications and Catalytic Synthesis. Carbon Resour Convers. 2021; 4:150–163.

7. Calvo GH, Cosenza VA, Sáenz DA, Navarro DA, Stortz CA, Céspedes MA, Mamone LA, Casas AG, Di Venosa GM. Disaccharides Obtained from Carrageenan as Potential Antitumor Agents. Sci Rep. 2019; 9:6654.
8. Yuan H, Song J, Li X, Li N, Dai J. Immunomodulation and Antitumor Activity of κ-Carrageenan Oligosaccharides. Pharmacol Res. 2006; 54(1):47–55.
9. Yustisia I, Hardjo M, Hasri, Sari WON, Kasmiati. Optimization and Characterization of *Kappaphycus alvarezii* and κ-Carrageenan Hydrolysates with Potential Biomedical Applications. Food Hydrocoll Health. 2025; 7:100205.
10. Panjaitan RS and Natalia L. Ekstraksi Polisakarida Sulfat Dari *Sargassum polycystum* Dengan Metode Microwave Assisted Extraction Dan Uji Toksisitasnya. JPB Kelautan Perikanan. 2021; 16(1):23–32.
11. Hernández-López A, Sánchez Félix DA, Zuñiga Sierra Z, García Bravo I, Dinkova TD, Avila-Alejandre AX. Quantification of Reducing Sugars Based on the Qualitative Technique of Benedict. ACS Omega. 2020; 5:32403–32410.
12. Kim S, Chen J, Cheng T, Gindulyte A, He J, He S, Li Q, Shoemaker BA, Thiessen PA, Yu B, Zaslavsky L, Zhang J, Bolton EE. PubChem in 2021: New Data Content and Improved Web Interfaces. Nucleic Acids Res. 2021; 49(D1):D1388–D1395.
13. Xiong G, Wu Z, Yi J, Fu L, Yang Z, Hsieh C, Yin M, Zeng X, Wu C, Lu A, Chen X, Hou T, Cao D. ADMETlab 2.0: An Integrated Online Platform for Accurate and Comprehensive Predictions of ADMET Properties. Nucleic Acids Res. 2021; 49(W1):W5–W14.
14. Filimonov DA, Lagunin AA, Gloriozova TA, Rudik AV, Druzhilovskii DS, Pogodin PV, Poroikov VV. Prediction of the Biological Activity Spectra of Organic Compounds Using the PASS Online Web Resource. Chem Heterocycl Compd. 2014; 50(3):444–457.
15. Ren X, Yan CX, Zhai RX, Xu K, Li H, Fu XJ. Comprehensive Survey of Target Prediction Web Servers for Traditional Chinese Medicine. Heliyon. 2023; 9:e19151.
16. Pati A, Gaur M, Sahu A, Subudhi BB, Kar D, Parida JR, Kuanar A. Drug Target Screening for Rheumatoid Arthritis by *Curcuma caesia* Through Computational Approach. Curr Plant Biol. 2025; 42:100468.
17. Hu M, Yan H, Li H, Feng Y, Sun W, Ren Y, Ma L, Zeng W, Huang F, Jiang Z, Dong H. Use of Network Pharmacology and Molecular Docking to Explore the Mechanism of Action of Curcuma in the Treatment of Osteosarcoma. Sci Rep. 2023; 13:9569.
18. Karima R, Elya B, Sauriasari R. Mechanism of Action of Glucomannan as a Potential Therapeutic Agent for Type 2 Diabetes Mellitus Based on Network Pharmacology and Molecular Docking Simulation. Trop J Nat Prod Res. 2023; 7(12):5460–5469.
19. Tang Z, Kang B, Li C, Chen T, Zhang Z. GEPIA2: An Enhanced Web Server for Large-Scale Expression Profiling and Interactive Analysis. Nucleic Acids Res. 2019; 47(W1):W556–W560.
20. Khotimah H, Hartiyo LB, Istiana S, Katili I, Jatmiko W. Prediction of Anti-Inflammatory Effects of *Rosmarinus officinalis L.* in Osteoarthritis Through Inhibition in PGE2-R, COX-2, and IL-1β: An *In Silico* Study. Trop J Nat Prod Res. 2025; 9(2):504–511.
21. Krylova NV, Kravchenko AO, Iunikhina OV, Pott AB, Likhatskaya GN, Volod'ko AV, Zaporozhets TS, Shchelkanov MY, Yermak IM. Influence of the Structural Features of Carrageenans From Red Algae of the Far Eastern Seas on Their Antiviral Properties. Mar Drugs. 2022; 20(1):60.
22. Usov AI. Polysaccharides of the Red Algae. Adv Carbohydr Chem Biochem. 2011; 65:115–217.
23. Liu J, Kandasamy S, Zhang J, Kirby CW, Karakach T, Hafting J, Critchley AT. Prebiotic Effects of Diet Supplemented with the Cultivated Red Seaweed *Chondrus crispus* or Its Isolated Polysaccharide Fraction in Rats. Front Microbiol. 2016; 7:826.
24. Cunha L and Grenha A. Sulfated Seaweed Polysaccharides as Multifunctional Materials in Drug Delivery Applications. Mar Drugs. 2016; 14(3):42.
25. Lipinski CA, Lombardo F, Dominy BW, Feeney PJ. Experimental and Computational Approaches to Estimate Solubility and Permeability in Drug Discovery and Development Settings. Adv Drug Deliv Rev. 2001; 46(1-3):3–26.
26. Tian X, Srinivasan PR, Tajiknia V, Sanchez Sevilla Uruchurtu AF, Seyhan AA, Carneiro BA, De La Cruz A, Pinho-Schwermann M, George A, Zhao S, Strandberg J, Di Cristofano F, Zhang S, Zhou L, Raufi AG, Navaraj A, Zhang Y, Verovkina N, Ghandali M, Ryspayeva D, El-Deiry WS. Targeting Apoptotic Pathways for Cancer Therapy. J Clin Invest. 2024; 134(14):e179570.
27. Levine AJ. p53: 800 Million Years of Evolution and 40 Years of Discovery. Nat Rev Cancer. 2020; 20:471–480.
28. Rawlings ND and Salvesen GS. Handbook of Proteolytic Enzymes. Academic Press; 2013.
29. Kushkevych I, Dordević D, Alberfkani MI, Gajdács M, Ostorházi E, Vítězová M, Rittmann SKMR. NADH and NADPH Peroxidases as Antioxidant Defense Mechanisms in Intestinal Sulfate-Reducing Bacteria. Sci Rep. 2023; 13:1.
30. Li S, Wang Q, Jia Z, Da M, Zhao J, Yang R, Chen D. Recent Advances in Glucose Oxidase-Based Nanocarriers for Tumor Targeting Therapy. Heliyon. 2023; 9(10):e20449.
31. Warburg O. On the Origin of Cancer Cells. Science. 1956; 123(3191):309–314.
32. Hanahan D and Weinberg RA. Hallmarks of Cancer: The Next Generation. Cell. 2011; 144(5):646–674.
33. Hoesel B and Schmid JA. Complexity of NF-κB Signaling in Inflammation and Cancer. Mol Cancer. 2013; 12:86.
34. Garg R, Benedetti LG, Abera MB, Wang H, Abba M, Kazanietz MG. Protein Kinase C and Cancer: What We Know and What We Don't. Oncogene. 2014; 33(45):5225–5237.
35. Pastorekova S and Gillies RJ. The Role of Carbonic Anhydrase IX in Cancer Development: Links to Hypoxia, Acidosis, and Beyond. Cancer Metastasis Rev. 2019; 38(1-2):65–77.
36. Lee AS. Glucose-Regulated Proteins in Cancer: Molecular Mechanisms and Therapeutic Potential. Nat Rev Cancer. 2014; 14(4):263–276.
37. Wang M and Kaufman RJ. Protein Misfolding in the Endoplasmic Reticulum as a Conduit to Human Disease. Nature. 2020; 529(7586):326–335.
38. Cerezo M and Rocchi S. New Anti-Cancer Molecules Targeting HSPA5/BiP to Induce Endoplasmic Reticulum Stress. Cancer Lett. 2017; 382(1):27–37.
39. Ruvolo PP. Galectin 3 is a Guardian of the Tumor Microenvironment. Biochim Biophys Acta Mol Cell Res. 2019; 1866(1):159–169.
40. Mathupala SP, Rempel A, Pedersen PL. Glucose Catabolism in Cancer Cells: Identification and Characterization of a Marked Activation Response of the Type II Hexokinase Gene to Hypoxic Conditions. J Biol Chem. 2001; 276(46):43407–43412.
41. Nath K, Guo L, Nancolas B, Nelson DS, Shestov AA, Lee SC, Roman J, Zhou R, Leeper DB, Halestrap AP, Blair IA, Glickson JD. Mechanism of Antineoplastic Activity of Lonidamine. Biochim Biophys Acta Rev Cancer. 2016; 1866(2):151–162.